Quantifying coherent and incoherent cathodoluminescence in semiconductors and metals

B. J. M. Brenny,[1] T. Coenen,[1] and A. Polman[1, a)]

Center for Nanophotonics, FOM Institute AMOLF, Science Park 104, 1098 XG Amsterdam, The Netherlands

We present a method to separate coherent and incoherent contributions to cathodoluminescence from bulk materials by using angle-resolved cathodoluminescence spectroscopy. Using 5 and 30 keV electrons we measure the cathodoluminescence spectra for Si, GaAs, Al, Ag, Au and Cu and determine the angular emission distributions for Al, GaAs and Si. Aluminium shows a clear dipolar radiation profile due to coherent transition radiation, while GaAs shows incoherent luminescence characterized by a Lambertian angular distribution. Silicon shows both transition radiation and incoherent radiation. From the angular data we determine the ratio between the two processes and decompose their spectra. This method provides a powerful way to separate different radiative cathodoluminescence processes, which is useful for material characterization and in studies of electron-matter and light-matter interaction in metals and semiconductors.

[a)] Electronic mail: polman@amolf.nl

I. INTRODUCTION

Cathodoluminescence (CL), the radiation excited by a ray of fast electrons, was first studied during the development of cathode tubes[1,2]. More detailed studies proliferated after the development of scanning electron microscopes (SEMs), first with a focus on mineralogy and petrology to identify geological samples by examining mineral-specific luminescence[3,4], later encompassing materials science in general[5,6]. One can study (band-gap) luminescence and other electron transitions across a broad range of energies[7–9]. The luminescent properties can be used to examine often inacessible details such as variations in the local composition, local dopant concentration, stress and strain, interfaces and non-radiative recombination centres such as point or extended defects[10–13]. One can also create and excite such defect states using electron irradiation to study their nature and behavior[14–17]. Cathodoluminescence studies of nanoscale structures are on the increase as well[18–21].

In the last decade, CL has gained attention among the nanophotonics community, mostly centered on studies of plasmonic systems, although studies on dielectrics are proliferating. Measuring with a nanoscale excitation probe, especially when combining spectral and angular data, turns CL into a very powerful tool. Optical antennas[22–29], plasmonic nanocavities[30,31], waveguides[32–34], and periodic crystals[35–37] amongst others have been examined to study their dispersion, radiation profiles, and spatial modal distributions.

A high energy electron beam can generate radiation in a material through a multitude of processes, which can be separated into coherent and incoherent groups[38]. Coherent radiation, so-called because the emitted radiation has a fixed phase relation with the electric field of the incident electron, comprises transition radiation (TR) at the surface, generation of plasmons, and Cherenkov radiation (when applicable). These processes can be used to probe the electromagnetic behavior of nanoscale objects with great precision, but are often quite weak. Nevertheless, TR and plasmon generation are the dominant processes in metals. Incoherent radiation such as luminescence generated by electron-hole recombination in semiconductors is usually much stronger and does not interfere with coherent radiation.

CL measurements for material science have generally consisted of spectral measurements, which are very powerful in determining characteristic optical resonances and transitions for a given material. However, if different radiative mechanisms are at play, it is often not possible to separate them. Here, we present the use of angle-resolved CL spectroscopy to

separate fundamental CL processes by their characteristic angular emission distributions. We investigate coherent TR and incoherent luminescence that each have very distinctive emission patterns, allowing us to discriminate between them and characterize them separately. We study Al, Ag, Au and Cu that show strong TR, and GaAs which shows strong incoherent luminescence. We then focus on partitioning TR and incoherent emission in Si, where we find that both mechanisms strongly contribute to the CL radiation.

II. EXPERIMENT

We performed measurements on polished p-type (B doping level $10^{15} - 10^{16}$ cm^{-3}) and n-type (P doping level 10^{15} cm^{-3}) single-crystal Si $\langle 100 \rangle$ wafers. No significant differences were found in CL measurements for these two sample types. A single-crystal wafer of Czochralski-grown Al was used to study TR and to characterize the system response of our setup. Layers of Au, Ag and Cu were grown on a silicon substrate by thermal evaporation. We used evaporation rates of 0.5 Å/s at a chamber pressure of $\sim 10^{-6}$ mbar. In each case the metal layers are at least 200 nm thick, such that they are optically thick. Finally, a single-crystal slab of GaAs was used as a model for a strongly incoherent emitting material. The dielectric functions of the metal films were measured using variable-angle spectroscopic ellipsometry and compared to values from Palik[39] or Johnson & Christy[40].

The experiments are all performed at room temperature in our Angle-Resolved Cathodoluminescence Imaging Spectroscopy (ARCIS) setup[41]. This consists of a FEI XL-30 SFEG scanning electron microscope (SEM) in which we place an aluminium paraboloid mirror that can be precisely positioned with a piezoelectric micromanipulation stage. We use the focused electron beam to generate radiation in our samples, which is collected by the mirror and directed out of the microscope to an optical detection system. For spectroscopy measurements we focus the light onto a fiber connected to a spectrometer with a liquid-nitrogen-cooled Si CCD photo-detector. Alternatively, we can image the parallel beam emanating from the paraboloid mirror onto a 2D Si CCD camera, which allows us to determine the angular emission profiles of the emitted radiation[41]. In this case each emission direction from the sample will hit the mirror at a specific location and be directed onto a specific point of the CCD camera. The 2D image is then transformed into a far-field angular radiation pattern. For the angular measurements we use color filters to select certain free-space wavelength

67 ranges (40 nm bandwidth filters, from $\lambda_0 = 400 - 900$ nm in 50 nm steps).

68 The spectral measurements on the single-crystal Al, evaporated Au, Ag and Cu were 69 performed at a beam energy of 30 keV and a current of approximately 15 nA. The integration 70 time varied between 0.5 and 4 s. Measurements on single-crystal Si were performed at 5 71 and 30 keV, with the same nominal current. Data from GaAs was collected at 30 keV, 72 but since the band-gap luminescence is extremely bright, we used a much lower current of 73 roughly 0.15 nA. CL count rates were linear with beam current in all cases. Spectral data 74 are corrected by subtracting the dark spectrum measured with the electron beam blanked, 75 which accounts for thermal and readout noise of the detector. During the measurement we 76 scan the beam over a 200×200 nm square area, in 20 nm steps. A spectrum is measured for 77 each pixel and the data is then averaged. We find measurements taken on different locations 78 on the samples are very consistent. The correction to account for the spectral sensitivity 79 of the system is described further on. For angular measurements, the same currents and 80 energies were used as for the spectral measurements, while the integration times were 60 s 81 for Al and Si, and 1 s for GaAs. For the angular data we took 2-3 measurements for each 82 filter wavelength in order to average them, and each measurement is corrected with a dark 83 measurement.

84 III. RESULTS AND DISCUSSION

85 A beam of highly energetic electrons can transfer its energy to a material or structure in 86 different ways, leading to a variety of radiative and non-radiative processes. Figure 1 gives 87 an overview of radiation processes one commonly encounters in most materials. The typical 88 behavior of metals is shown in (a), where coherent processes such as TR and generation of 89 surface plasmons polaritions (SPPs) are dominant[38,42]. Due to fast non-radiative recombi- 90 nation of the free electrons, the beam does not tend to excite incoherent luminescence in 91 metals. SPPs can be excited efficiently on a flat surface, but as they cannot radiate to the 92 far field for an unstructured planar surface, the only contribution to measured radiation is 93 from TR, which has a toroidal emission pattern similar to that of a vertical point dipole 94 at the surface as shown in Figure 1(a)[38,41,42]. The cartoon on the right shows a simplified 95 visualization of this process: the negatively charged electron induces a positive mirror charge 96 in the metal that disappears when the electron transits the interface. The corresponding

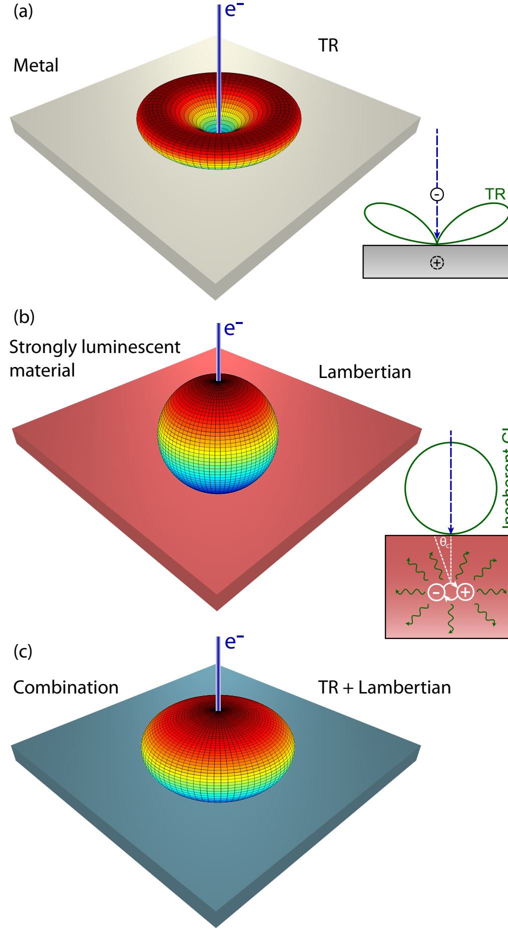

FIG. 1. (a) Schematic angular emission profile for electron-beam induced radiation from a metal, which is dominated by TR. The cartoon on the right sketches this process, where the electron creates an image charge in the metal, giving rise to a vertical dipole at the surface which emits radiation with a toroidal angular shape. (b) Schematic angular emission profile for incoherent luminescence generated inside the material with a Lambertian emission profile. The cartoon on the right shows electron-hole recombination emitting light isotropically, only light emitted within the critical angle escapes from the sample. (c) Schematic emission profile for a combination of TR and luminescence, which is the case for Si. The profile is an average of those from (a) and (b).

97 varying dipole moment then leads to radiation into the far field with an angular emission
98 profile very similar to that of a radiating point dipole placed just above the metal surface.
99 For dielectrics, the corresponding picture contains a polarisation charge with a magnitude
100 determined by the dielectric constant, and TR generation occurs as well[38].

101 In the case of many semiconductors and dielectrics, incoherent luminescence is the main
102 source of radiation as it is usually orders of magnitude stronger than coherent emission such
103 as TR. A schematic of such a luminescent material is shown in Figure 1(b). The ener-
104 getic electron can excite a material to a range of excited states over a very broad spectral
105 range. The impact excitation cross sections for these transitions are higher than many op-
106 tical excitation cross sections, and, because of the high incident energy and the formation
107 of an electron cascade, a single incident electron can lead to multiple material excitations.
108 Creation of an electron-hole pair by an incident electron typically requires a few times the
109 energy of the band-gap[43,44], so excitations in the visible and infrared can be generated by
110 both the primary and secondary electrons. The low-energy secondary electrons and deceler-
111 ated incident electrons have higher excitation cross sections than the primary electrons, as
112 their localized fields can couple more strongly to such excitations than the more delocalized
113 fields of fast electrons[38]. As this kind of CL radiation is caused by spontaneous emission,
114 it is not coherent with the electric field of the incident electron and will not interfere with
115 radiation that is coherent such as TR. The emission is usually due to the radiative recom-
116 bination of electron-hole pairs and excitons which can recombine to the ground state or to
117 intermediate excited defect states, which then decay to the ground state through radiative
118 or non-radiative pathways. Incoherent emission typically occurs isotropically inside a ma-
119 terial. The resulting CL emission distribution exiting the material is Lambertian, whith a
120 cosine dependence on the zenithal angle, as shown in Figure 1(b). The cosine dependence
121 occurs due to the refraction of light and follows directly from Snell's law[45]. The cartoon in
122 Figure 1(b) illustrates these processes, and also indicates the critical angle beyond which
123 radiation is fully reflected into the substrate. Figure 1(c) shows a schematic of the emission
124 pattern determined by a combination of TR and Lambertian profiles. Next, we present the
125 experimental spectra and angular emission profiles for each of the three cases described here.
126 We use Al as a TR emitter, GaAs as a strong incoherent emitter, and Si representing both
127 effects.

128 Figure 2(a) shows the CL spectra from bulk crystals of Al, GaAs and Si at 30 keV.
129 Data for Si at 5 keV are also shown. We observe that the Al and Si spectra show similar,
130 broadband spectral shapes while the GaAs spectrum is much sharper and peaks at about
131 $\lambda_0 = 870$ nm, corresponding to the band gap energy ($\sim$1.43 eV, or $\sim$867 nm, at 300 K).

132 Figure 2(b) shows the calculated TR spectra for the same three materials, where the TR

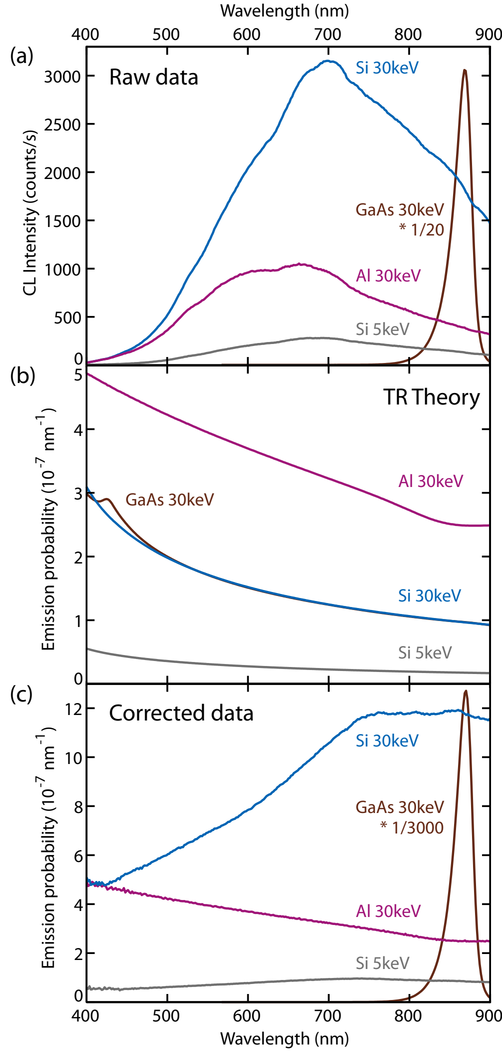

FIG. 2. (a) Measured cathodoluminescence spectra from bulk samples of single crystalline Al, GaAs and Si. Data was taken at 30 keV; for silicon also at 5 keV. The beam current for Al and Si was 15 nA, for GaAs 0.15 nA. The GaAs spectrum is divided by a factor of 20. (b) Calculated TR emission probability as a function of wavelength for Al, GaAs and Si. (c) The spectra of Al, GaAs and Si corrected by the system response using the TR data for Al as a reference. In this case the GaAs spectrum is divided by a factor of 3000.

133 intensity is expressed in units of photon emission probability per incoming electron per unit
134 bandwidth. The calculation is based on the theoretical formalism described in section IV.C
135 of Ref. 38. In this approach Maxwell's equations are solved for a swift electron interacting
136 with a material, more specifically the case of an electron normally incident on a planar

137 substrate. The moving charge induces surface charges and currents that lead to a reflected
138 electromagnetic field at the surface that is the source of TR. The emitted TR is angle and
139 wavelength dependent, so one can obtain angular intensity distributions and determine the
140 total spectrum by performing the angular integral over the upper hemisphere. The variables
141 that are of importance for the wavelength and amplitude dependence of the TR are the
142 electron energy, beam current and material permittivity. The electron energy affects the TR
143 amplitude because a higher energy electron has electric fields that extend further from its
144 trajectory, and can thus polarize a larger volume of material, inducing more surface currents
145 and increasing the TR response. The TR intensity is given by an emission probability per
146 electron, so the signal increases linearly with the number of electrons. In this way the
147 beam current only affects the amplitude, and does so in constant fashion for all wavelengths
148 leading to a fixed factor difference in the spectrum. As far as the wavelength dependence is
149 concerned, TR is an interface effect based on the reflection of induced fields, so the equations
150 contain information about light dispersion in both media, in a way similar to that of the
151 Fresnel equations. Since in our case one medium is vacuum, the material permittivity of the
152 sample determines the wavelength dependence of TR. Spectral features can be correlated
153 with features in the permittivity. We use optical constants measured by ellipsometry for Al
154 and an average of tabulated values for Si and GaAs. The inset in Figure 3 compares the real
155 and imaginary part of the permittivity of Al that we measured by ellipsometry with values
156 from Palik[39]. The trends are similar, but the absolute values of both real and imaginary
157 parts of the permittivity differ; we attribute this to differences between the density and
158 crystallinity of our single crystal compared to samples used by Palik. We can see that the
159 calculated spectra for all three materials follow the same trends as their dielectric function.
160 The TR spectra of GaAs and Si are quite similar, in agreement with the similar permittivity.
161 We also note that using a lower electron energy leads to a lower TR emission probability for
162 Si.

163 As the CL signal from Al is purely due to TR, we now use it to calibrate our setup and
164 determine the (relative) system response due to the spectral sensitivity of the setup. This
165 will allow us to normalize the other experimental spectra. We obtain this system response
166 by dividing the theoretical TR spectrum by the measured spectrum from the single crystal
167 Al. We can then multiply the other measured spectra by this correction factor to obtain the
168 emission probabilities for the other materials.

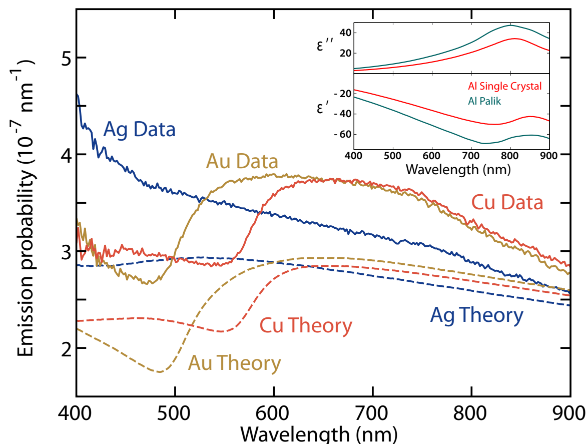

FIG. 3. Cathodoluminescence spectra of evaporated Au, Ag and Cu that have been corrected for the system response (solid curves), compared to the calculated TR spectra (dashed curves). The inset shows the real and imaginary part of the permittivity of Al measured using ellipsometry together with values from Palik[39].

169 Figure 2(c) shows the corrected CL spectra for Al, GaAs and Si. Clearly, the corrected 170 Si spectrum at 30 keV does not correspond to the theoretical TR spectrum in Figure 2(b) 171 at all, as the spectral shape is quite different and the intensities are $2-12$ times higher than 172 the TR spectrum. At 5 keV, the corrected spectrum for Si also exceeds the TR spectrum. 173 It is clear that the Si spectrum cannot be explained as being only due to TR, and since 174 Si is a semiconductor, incoherent radiative processes must play a role even if non-radiative 175 recombination is dominant. We do not expect Cherenkov radiation to play a role even 176 though the refractive index is high enough to satisfy the emission condition, because it is 177 emitted in the forward direction downwards into the substrate where it is fully absorbed.

178 In Figure 3, we examine the CL spectra of Au, Ag and Cu, for which we expect the 179 spectrum to be dominated by TR. The measured spectra are corrected using TR data from 180 Al in the same way as above. Theoretical TR spectra of Au, Ag and Cu are also shown as 181 comparison. Several trends can be observed. First of all, the experimental TR spectra for 182 Au, Ag and Cu have quite similar intensities, with clear kinks in the spectra for Au and Cu 183 at $\lambda_0 = 500$ and 550 nm respectively. The theoretical spectra show similar trends, the kinks 184 for Au and Cu occur at the same wavelengths as for the experimental spectra. The absolute 185 emission probabilities do not agree well between experiment and theory; they differ by up to

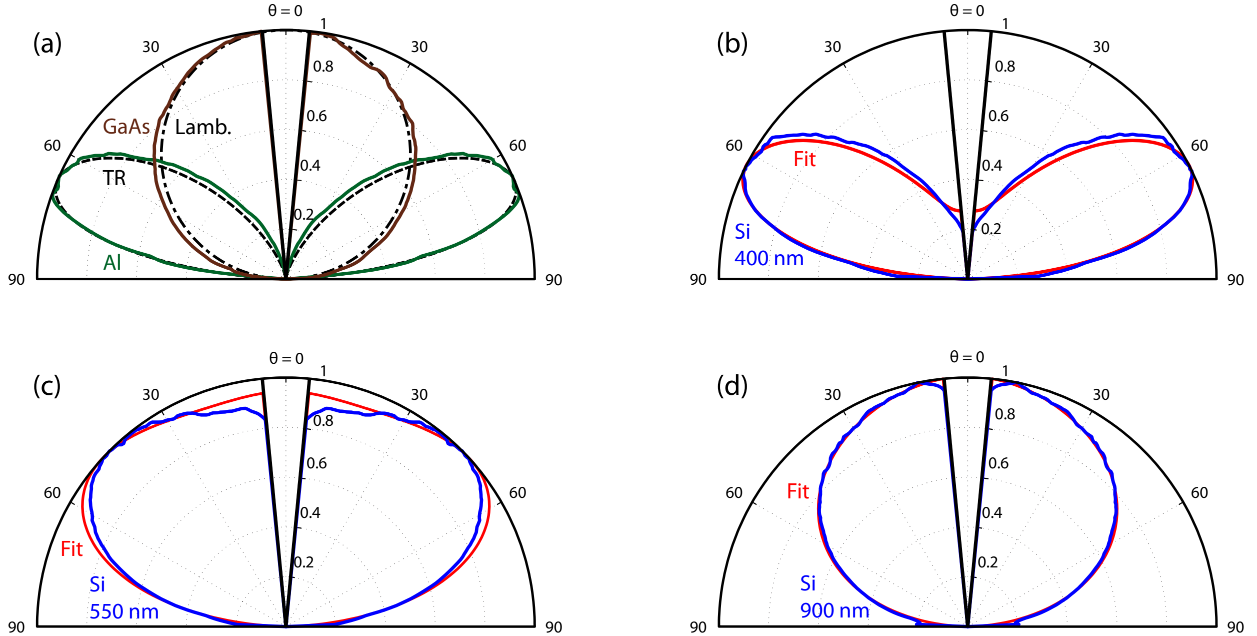

FIG. 4. (a) Measured normalized emission patterns as a function of polar angle θ for Al and GaAs (solid lines, measured at 400 and 850 nm, respectively). The theoretical TR pattern for Al and a Lambertian pattern for GaAs are also shown (dashed lines). (b-d) Measured emission patterns of Si at 30 keV for 400, 550 and 900 nm (blue lines) and fits consisting of a combination of Lambertian and TR patterns (red lines).

186 ~ 30 %. We attribute this to variations between measurement sessions of the beam current,
187 as explained in the description of Figure 2(b), as well as changes in the system alignment
188 that affect the collection efficiency and thus the intensity. Repeated measurements with the
189 same sample and measurement conditions have shown one can indeed obtain up to ~ 30 %
190 variations in intensity. Because all of the data is normalized to the intensity of Al, differences
191 in current compared to that of the reference measurement will lead to an offset factor in the
192 spectrum. In this case the current was higher for the measurements than for the reference,
193 so the experimental spectra are a factor higher than the theoretical values. These results
194 show that overall, the experimental data well represent the theoretical spectral features.

195 Next, we study the angular emission profiles for Al, GaAs and Si at 30 keV. We find that
196 the radiation profiles are azimuthally symmetric and average the data over an azimuthal
197 range to obtain the polar profiles shown in Figure 4. Averaging was done over the azimuthal

198 angle ranges $\phi = 60 - 120°$ and $\phi = 240 - 300°$, where $\phi = 0/360°$ is the center of the
199 mirror's open end and $\phi = 180°$ corresponds to the apex at the back of the mirror. We
200 use these ranges to avoid the open end of the mirror and the apex which contains more
201 aberrations. To further decrease the noise for Al and Si we average the data obtained from
202 the two angular ranges. All angular distributions are normalized to 1; no data is collected in
203 the angular range $\theta = \pm 5°$ corresponding to the hole in the parabolic mirror. The angular
204 resolution is affected by the curvature of the mirror which modifies the solid angle of the
205 emitted radiation compared to its distribution on the CCD camera. As described in Ref. 41
206 (Fig 2.c), the solid angle per pixel varies between $(2 - 10) \times 10^{-5}$ sr.

207 Figure 4(a) shows angular profiles for Al (at $\lambda_0 = 400$ nm) and GaAs (at $\lambda_0 = 850$ nm)
208 together with theoretical curves for TR (Al) and a Lambertian emitter (GaAs). For Al,
209 the measured and calculated data agree very well, with the experimental one being slightly
210 broader, proving the emission from Al is well described by TR. The emission pattern from
211 GaAs corresponds well to the Lambertian profile, confirming that CL from GaAs at the
212 band gap energy is dominated by incoherent luminescence.

213 Figure 4(b-d) shows the experimental angular profiles for Si at 30 keV, measured at
214 $\lambda_0 = 400$, 550 and 900 nm, respectively. Clearly, at $\lambda_0 = 400$ nm the emission pattern is
215 more TR-like while it becomes more Lambertian-like and thus dominated by luminescence
216 for the longer wavelengths.

217 For the case of incoherent luminescence it is important to keep in mind that carrier
218 transport can play a role in determining the emission properties. Diffusion as well as photon
219 recycling can lead to recombination well outside the area of initial generation by the electron
220 beam. Additionaly, carrier transport can be anisotropic, further impacting the distribution
221 of recombination and thus affecting the resulting spatial and angular CL profiles[46]. In our
222 case there is very good agreement with the Lambertian profile, so we expect that these
223 effects play a minor role.

224 To determine the relative contributions of the two processes and separate them, we model
225 the emission pattern as a linear combination of TR and Lambertian profiles for the given
226 wavelengths, with the relative contributions as fit parameters in a least squares fitting rou-
227 tine. The fitted angular profiles are shown in red in Figure 4(b-d) and agree well with the
228 measured data. Next, we extend this analysis to the full $400 - 900$ nm spectral range in
229 steps of 50 nm, both for 30 and 5 keV electron energies. The relative contributions of TR

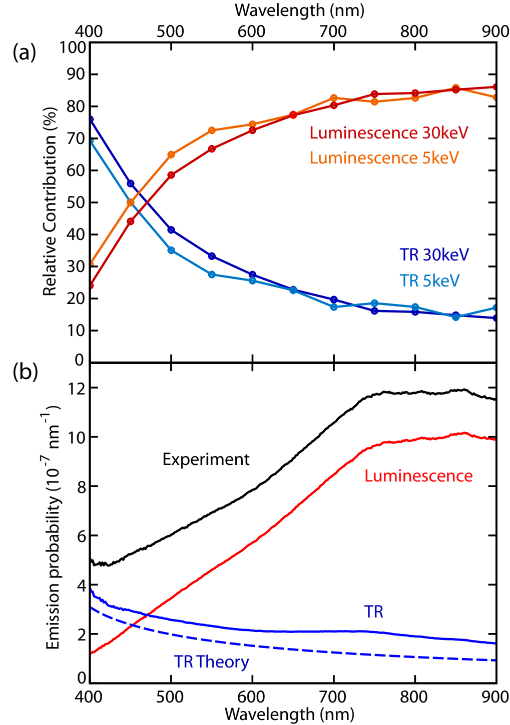

FIG. 5. (a) Relative contributions of TR and luminescence derived from fits to the Si emission patterns as in Figure 4, both for 5 and 30 keV electron energy (circles). The drawn lines are a guide to the eye. The circles show the data points. (b) The CL spectrum from Figure 2(c) (black) together with TR (blue) and incoherent luminescence (red) contributions for Si at 30 keV derived using the fractions from (a). The theoretical TR spectrum for Si at 30 keV is shown as well (blue dashed line).

230 and incoherent radiation is then determined from the fits for each wavelength; the result is
231 shown in Figure 5(a). TR dominates at the shorter wavelengths, while incoherent emission
232 dominates at longer wavelengths. Similar trends are observed for 5 and 30 keV. The transi-
233 tion in dominance between the two radiative mechanisms is due to a combination of effects.
234 TR has an increased intensity at shorter wavelengths as one can see from the calculation in
235 Figure 2(b), while luminescence which is emitted inside the material will be absorbed much
236 more strongly for short wavelengths than for long wavelengths, so more ”red” luminescence
237 will escape the Si.

238 Now that we have determined the relative contributions of these two radiative processes
239 in Si, we can use this information to decompose the TR and incoherent luminescence spectra.

240 We fit a smooth curve through the data points in Figure 5(a) and use this to partition the
241 experimental spectrum for Si at 30 keV from Figure 2(c). The total spectrum for Si at 30
242 keV as well as the separated TR and incoherent contributions are shown in Figure 5(b).
243 Comparing the experimentally determined TR contribution with the calculation, the overal
244 behavior as a function of wavelength is well reproduced, while the absolute intensities differ
245 by a factor ~ 1.5 which we attribute to a difference in beam current, as was discussed earlier.

246 Figure 5(b) shows that the incoherent Si spectrum is spectrally broad, peaks for $\lambda_0 > 750$
247 nm and extends above the TR spectrum for $\lambda_0 > 470$ nm. We attribute this incoherent
248 spectrum to transitions between defect states in the direct band gap. Since n-type and p-
249 type samples gave similar results, doping-related luminescence is insignificant. We note that
250 light emission is strongly absorbed in Si, especially in the blue, so the collected spectrum
251 does not directly reflect the emitted incoherent spectrum. Correcting for this effect the
252 relative contribution emitted in the blue spectral range is larger than what is observed in
253 the measured spectrum.

254 Our data can be compared with experiments at 200 keV performed by Yamamoto et. al.[47]
255 at 200 keV in which the CL spectrum from Si closely follows the calculated TR spectrum,
256 with no discernible incoherent radiation. This is due to the fact that the TR intensity is ~6
257 times stronger at 200 keV than at 30 keV. Moreover, at 200 keV the penetration depth of
258 the electrons is much larger than at 30 keV (up to ~200 μm versus ~10 μm)[48,49]. Since the
259 incoherent radiation is generated more efficiently as the electrons have decelerated deeper
260 inside the material, it will be strongly absorbed inside the Si for higher electron energies.

261 **IV. CONCLUSIONS**

262 We demonstrated a method to distinguish coherent and incoherent cathodoluminescence
263 processes induced by a beam of fast electrons. We have shown that Al exhibits coher-
264 ent transition radiation, while GaAs exhibits mainly incoherent band-gap luminescence. Si
265 cathodoluminescence is composed of both transition radiation and incoherent radiation. We
266 distinguish the two processes by their characteristic angular profiles, namely dipolar-like
267 lobes for transition radiation and a Lambertian angular distribution for incoherent lumines-
268 cence. For silicon at 5 and 30 keV, transition radiation dominates around $\lambda_0 = 400$ nm,
269 making up ~70 % of the signal while incoherent luminescence becomes increasingly stronger

for longer wavelengths, consisting of ∼85 % of the signal at $\lambda_0 = 900$ nm. Determining the relative strengths of these two effects allows us to decompose the experimental Si cathodoluminescence spectrum to retrieve the spectrum due to transition radiation, which agrees with calculations, and the spectrum due to luminescence, which is very broadband. Using angle-resolved cathodoluminescence to identify, separate and characterize different coherent and incoherent radiative processes is a powerful way to quantify such different forms of radiation in a multitude of materials such as metals and semiconductors. The technique is quite flexible in separating different radiative mechanisms, so long as one measures processes that do not interfere with each other (or do so in a way that can easily be deconvoluted) and have differing angular distributions. The use of antennas, (nano)structured surfaces or non-planar surfaces can all modify the coherent or incoherent distributions, but often in ways that are predictable by calculation or simulation. One can then use the modified angular patterns to separate the processes. For example, a luminescent sample with a hemispherical instead of planar surface will not display a Lambertian but a hemispherical angular distribution due to incoherent luminescence. Alternatively, one could separate the coherent emission of an antenna from the luminescence of the substrate. The presented results are relevant for material characterization and for studies of electron-matter and light-matter interaction in general.

V. ACKNOWLEDGMENTS

We would like to acknowledge Andries Lof and Hans Zeijlemaker for technical support, as well as Arkabrata Bhattacharya and Hemant Tyagi for providing us with the GaAs samples. This work is part of the research program of the "Stichting voor Fundamenteel Onderzoek der Materie (FOM)", which is financially supported by the "Nederlandse Organisatie voor Wetenschappelijk Onderzoek (NWO)". This work is part of NanoNextNL, a nanotechnology program funded by the Dutch ministry of economic affairs. It is also supported by the European Research Council (ERC).

REFERENCES

[1]W. Crookes, Phil. Trans. **170**, 641 (1879).

298 [2]T. Arabatzis, in *Compendium of Quantum Physics*, edited by D. Greenberger, K. Hentschel, and F. Weinert (Springer Berlin Heidelberg, 2009) pp. 89–92.
300 [3]M. Pagel, V. Barbin, P. Blanc, and D. Ohnenstetter, *Cathodoluminescence in geosciences* (Springer, 2000).
302 [4]D. J. Marshall and A. N. Mariano, *Cathodoluminescence of geological materials* (Unwin Hyman Boston etc., 1988).
304 [5]S. Myhajlenko, *Luminescence of Solids*, edited by D. R. Vij (Springer US, 1998) pp. 135–188.
306 [6]B. Yacobi and D. Holt, J. Appl. Phys. **59**, R1 (1986).
307 [7]R. Sauer, H. Sternschulte, S. Wahl, K. Thonke, and T. R. Anthony, Phys. Rev. Lett. **84**, 4172 (2000).
309 [8]S. Koizumi, K. Watanabe, M. Hasegawa, and H. Kanda, Science **292**, 1899 (2001).
310 [9]G. Li, D. Geng, M. Shang, C. Peng, Z. Cheng, and J. Lin, J. Mater. Chem. **21**, 13334 (2011).
312 [10]K. Thonke, I. Tischer, M. Hocker, M. Schirra, K. Fujan, M. Wiedenmann, R. Schneider, M. Frey, and M. Feneberg, IOP Conf. Ser.: Mater. Sci. Eng. **55**, 012018 (2014).
314 [11]P. R. Edwards and R. W. Martin, Semicond. Sci. Technol. **26**, 064005 (2011).
315 [12]B. Dierre, X. Yuan, and T. Sekiguchi, Sci. Technol. Adv. Mater. **11**, 043001 (2010).
316 [13]A. Leto and G. Pezzotti, Phys. Status Solidi A **208**, 1119 (2011).
317 [14]M. Avella, J. Jiménez, F. Pommereau, J. Landesman, and A. Rhallabi, Mat. Sci. Eng. B **147**, 136 (2008).
319 [15]C. Ton-That, L. Weston, and M. Phillips, Phys. Rev. B **86** (2012).
320 [16]F. A. Ponce, D. P. Bour, W. Götz, and P. J. Wright, Appl. Phys. Lett. **68**, 57 (1996).
321 [17]H.-J. Fitting, A. N. Trukhin, T. Barfels, B. Schmidt, and A. V. Czarnowski, Radiat. Eff. Defect. S. **157**, 575 (2002).
323 [18]D. Spirkoska, J. Arbiol, A. Gustafsson, S. Conesa-Boj, F. Glas, I. Zardo, M. Heigoldt, M. Gass, A. Bleloch, S. Estrade, M. Kaniber, J. Rossler, F. Peiro, J. Morante, G. Abstreiter, L. Samuelson, and A. Fontcuberta I Morral, Phys. Rev. B **80** (2009).
326 [19]L. H. G. Tizei and M. Kociak, Phys. Rev. Lett. **110**, 153604 (2013).
327 [20]C.-W. Chen, K.-H. Chen, C.-H. Shen, A. Ganguly, L.-C. Chen, J.-J. Wu, H.-I. Wen, and W.-F. Pong, Applied Physics Letters **88**, 241905 (2006).

[21] Z. Mahfoud, A. T. Dijksman, C. Javaux, P. Bassoul, A. L. Baudrion, J. Plain, B. Dubertret, and M. Kociak, J. Phys. Chem. Lett. **4**, 4090 (2013).
[22] L. Novotny and N. van Hulst, Nat. Photonics **5**, 83 (2011).
[23] V. Myroshnychenko, J. Nelayah, G. Adamo, N. Geuquet, J. Rodríguez-Fernández, I. Pastoriza-Santos, K. F. MacDonald, L. Henrard, L. M. Liz-Marzán, N. I. Zheludev, M. Kociak, and F. J. García de Abajo, Nano Lett. **12**, 4172 (2012).
[24] M. W. Knight, L. Liu, Y. Wang, L. Brown, S. Mukherjee, N. S. King, H. O. Everitt, P. Nordlander, and N. J. Halas, Nano Lett. **12**, 6000 (2012).
[25] A. I. Denisyuk, G. Adamo, K. F. MacDonald, J. Edgar, M. D. Arnold, V. Myroshnychenko, J. Ford, F. J. García de Abajo, and N. I. Zheludev, Nano Lett. **10**, 3250 (2010).
[26] T. Coenen, F. Bernal Arango, A. F. Koenderink, and A. Polman, Nat. Commun. **5**, 3250 (2014).
[27] T. Coenen, E. J. R. Vesseur, A. Polman, and A. F. Koenderink, Nano Lett. **11**, 3779 (2011).
[28] A. Kumar, K.-H. Fung, J. C. Mabon, E. Chow, and N. X. Fang, J. Vac. Sci. Technol. B **28**, C6C21 (2010).
[29] E. J. R. Vesseur and A. Polman, Nano Lett. **11**, 5524 (2011).
[30] X. L. Zhu, J. S. Ma, Y. Zhang, X. F. Xu, J. Wu, Y. Zhang, X. B. Han, Q. Fu, Z. M. Liao, L. Chen, and D. P. Yu, Phys. Rev. Lett. **105**, 127402 (2010).
[31] M. Kuttge, F. J. G. de Abajo, and A. Polman, Opt. Express **17**, 10385 (2009).
[32] N. Yamamoto, S. Bhunia, and Y. Wantanabe, Appl. Phys. Lett. **88**, 154106 (2006).
[33] E. J. R. Vesseur, T. Coenen, H. Caglayan, N. Engheta, and A. Polman, Phys. Rev. Lett. **110**, 013902 (2013).
[34] A. C. Narváez, I. G. C. Weppelman, R. J. Moerland, N. Liv, A. C. Zonnevylle, P. Kruit, and J. P. Hoogenboom, Opt. Express **21**, 29968 (2013).
[35] R. Sapienza, T. Coenen, J. Renger, M. Kuttge, N. F. van Hulst, and A. Polman, Nat. Mater. **11**, 781 (2012).
[36] T. Suzuki and N. Yamamoto, Opt. Express **17**, 23664 (2009).
[37] K. Takeuchi and N. Yamamoto, Opt. Express **19**, 12365 (2011).
[38] F. J. García de Abajo, Rev. Mod. Phys. **82**, 209 (2010).
[39] E. D. Palik, *Handbook of optical constants* (Academic Press, New York, 1985).
[40] P. B. Johnson and R. W. Christy, Phys. Rev. B **6**, 43704379 (1972).

361 [41]T. Coenen, E. J. R. Vesseur, and A. Polman, Appl. Phys. Lett. **99**, 143103 (2011).
362 [42]M. Kuttge, E. J. R. Vesseur, A. F. Koenderink, H. J. Lezec, H. A. Atwater, F. J. García de
363 Abajo, and A. Polman, Phys. Rev. B **79**, 113405 (2009).
364 [43]T. E. Everhart and P. H. Hoff, J. Appl. Phys. **42**, 5837 (1971).
365 [44]C. A. Klein, J. Appl. Phys. **39**, 2029 (1968).
366 [45]E. F. Schubert, *Light emitting diodes, 2nd edition* (Cambridge University press, 2006).
367 [46]N. M. Haegel, T. J. Mills, M. Talmadge, C. Scandrett, C. L. Frenzen, H. Yoon, C. M.
368 Fetzer, and R. R. King, Journal of Applied Physics **105**, 023711 (2009).
369 [47]N. Yamamoto, A. Toda, and K. Araya, J. Electron Microsc. **45**, 64 (1996).
370 [48]D. Drouin, A. R. Couture, D. Joly, X. Tastet, V. Aimez, and R. Gauvin, Scanning **29**, 92
371 (2007).
372 [49]Casino Software, http://www.gel.usherbrooke.ca/casino/.